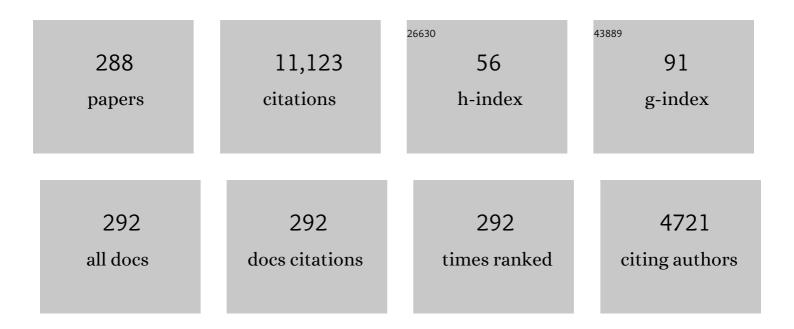
List of Publications by Year in descending order

Source: https://exaly.com/author-pdf/9058544/publications.pdf Version: 2024-02-01



#	Article	IF	CITATIONS
1	Textural and compositional evolution of niobium minerals in the Miaoya carbonatite-hosted REE-Nb deposit from the South Qinling Orogen of central China. Mineralium Deposita, 2023, 58, 197-220.	4.1	12
2	Genesis of the Hebaoshan gold deposit in Fujian Province of Southeast China: constraints from a combined fluid inclusion, H-O-C-S-Pb-He-Ar isotope and geochronological study. Mineralium Deposita, 2022, 57, 13-34.	4.1	12
3	Application of Raman spectroscopy for the identification of phosphate minerals from REE supergene deposit. Journal of Raman Spectroscopy, 2022, 53, 485-496.	2.5	11
4	In situ chemical and isotopic analyses and element mapping of multiple-generation pyrite: Evidence of episodic gold mobilization and deposition for the Qiucun epithermal gold deposit in Southeast China. American Mineralogist, 2022, 107, 1133-1148.	1.9	15
5	Age and fluid source of the sub-volcanic Zhaiping Ag–Pb–Zn deposit in the eastern Cathaysia Block (Fujian Province, Southeastern China). Mineralium Deposita, 2022, 57, 439-454.	4.1	2
6	Timing and tectonic setting of tin mineralization in southern Myanmar: constraints from cassiterite and wolframite U–Pb ages. Mineralium Deposita, 2022, 57, 977-999.	4.1	12
7	Neoproterozoic and Paleozoic tectonic evolution in north Qaidam, northeastern Tibetan Plateau recorded by magmatism and metamorphism. Gondwana Research, 2022, 103, 84-104.	6.0	6
8	Metallogeny of the Late Jurassic Qiucun epithermal gold deposit in southeastern China: Constraints from geochronology, fluid inclusions, and H-O-C-Pb isotopes. Ore Geology Reviews, 2022, 142, 104688.	2.7	10
9	U–Pb geochronology of columbite-group mineral, cassiterite, and zircon and Hf isotopes for Devonian rare-metal pegmatite in the Nanyangshan deposit, North Qinling Orogenic Belt, China. Ore Geology Reviews, 2022, 140, 104634.	2.7	5
10	Apatite chemistry as a petrogenetic–metallogenic indicator for skarn ore-related granitoids: an example from the Daye Fe–Cu–(Au–Mo–W) district, Eastern China. Contributions To Mineralogy and Petrology, 2022, 177, 1.	3.1	15
11	Silver isotope fractionation in ore-forming hydrothermal systems. Geochimica Et Cosmochimica Acta, 2022, 322, 24-42.	3.9	5
12	Titanite U-Pb dating and geochemical constraints on the Paleozoic magmatic-metamorphic events and Nb-Ta mineralization in the Yushishan deposit, South Qilian, NW China. Lithos, 2022, 412-413, 106612.	1.4	4
13	Deciphering multiple ore-forming processes of the Shuangqishan orogenic gold deposit, Southeast China by in situ analysis of pyrite. Ore Geology Reviews, 2022, 142, 104730.	2.7	9
14	Petrogenesis of Ta-Nb mineralization related Early Cretaceous Lingshan granite complex, Jiangxi Province, southeast China: Constraints from geochronology, whole-rock and in-situ mineral geochemistry, and Nd-Hf isotopic compositions. Ore Geology Reviews, 2022, 143, 104788.	2.7	5
15	Geochemistry of Ca-(K)-(Na) silicates from charoitites in the Sirenevyi Kamen gemstone deposit, Murun Complex, Eastern Siberia. Ore Geology Reviews, 2022, 143, 104787.	2.7	2
16	Fluid inclusion and stable isotope (C–H-O-S) constraints on the genesis of the Heilongtan-Xiejiagou Au deposit, northern Hubei, China. Ore Geology Reviews, 2022, 144, 104841.	2.7	4
17	Mineral paragenesis in Paleozoic manganese ore deposits: Depositional versus post-depositional formation processes. Geochimica Et Cosmochimica Acta, 2022, 325, 65-86.	3.9	8
18	Episodic emplacement of the Lingshan Granitic Complex and related two-stage molybdenum mineralization in the Dabie orogenic belt. Ore Geology Reviews, 2022, 144, 104820.	2.7	2

#	Article	IF	CITATIONS
19	LA-(MC)-ICP-MS U-Th-Pb dating and Nd isotopes of allanite in NYF pegmatite from lesser qingling orogenic belt, central China. Ore Geology Reviews, 2022, 145, 104893.	2.7	4
20	Early Cretaceous ocean-island basalt-type magmatism in northern Guangdong: implications for lithospheric thinning in the South China Block. Journal of the Geological Society, 2022, 179, .	2.1	1
21	Genesis of the Maogongdong deposit in the Dahutang W-Cu-(Mo) ore field of northern Jiangxi Province, South China: constraints from mineralogy, fluid inclusions, and H-O-C-S isotopes. Mineralium Deposita, 2022, 57, 1449-1468.	4.1	8
22	Trace element and S-Pb isotopic compositions of pyrite from the Precambrian metamorphic rocks and their derivative pegmatites in the Xiaoqinling district, southern North China Craton: Implications for possible gold source of the Early Cretaceous gold deposits. Precambrian Research, 2022, 377, 106739.	2.7	1
23	Textural features and in situ trace element analysis of fluorite from the Wujianfang fluorite deposit, Inner Mongolia (NE China): Insights into fluid metasomatism and ore-forming process. Ore Geology Reviews, 2022, 147, 104982.	2.7	3
24	Ore genesis of the Baishawo Be-Li-Nb-Ta deposit in the northeast Hunan Province, south China: Evidence from geological, geochemical, and U-Pb and Re-Os geochronologic data. Ore Geology Reviews, 2021, 129, 103895.	2.7	16
25	Geochronology and textural and compositional complexity of apatite from the mineralization-related granites in the world-class Zhuxi W-Cu skarn deposit: A record of magma evolution and W enrichment in the magmatic system. Ore Geology Reviews, 2021, 128, 103885.	2.7	19
26	lsotope evidence for multiple sources of B and Cl in Middle Miocene (Badenian) evaporites, Carpathian Mountains. Applied Geochemistry, 2021, 124, 104819.	3.0	3
27	Early Paleozoic Orogenic Gold Deposit in the Cathaysia Block, China: A first example from the Shuangqishan Deposit. Gondwana Research, 2021, 91, 231-253.	6.0	13
28	Middle Triassic diorites from the Loei Fold Belt, NE Thailand: Petrogenesis and tectonic implications in the context of Paleotethyan subduction. Lithos, 2021, 382-383, 105955.	1.4	8
29	Chemical and boron isotopic compositions of tourmaline at the Dachang Sn-polymetallic ore district in South China: Constraints on the origin and evolution of hydrothermal fluids. Mineralium Deposita, 2021, 56, 1589-1608.	4.1	26
30	Boron coordination and B/Si ordering controls over equilibrium boron isotope fractionation among minerals, melts, and fluids. Chemical Geology, 2021, 561, 120030.	3.3	18
31	Geochronological, geochemical, and <scp>Sr–Nd–Pb–Hf</scp> isotopes of Cretaceous gneissic granite and quartz monzonite in the Tongbai Complex: Record of lower crust thickening beneath the Tongbai orogen. Geological Journal, 2021, 56, 4126-4149.	1.3	Ο
32	Magmatic-hydrothermal processes and controls on rare-metal enrichment of the Baerzhe peralkaline granitic pluton, inner Mongolia, northeastern China. Ore Geology Reviews, 2021, 131, 103984.	2.7	12
33	Ore genesis of Qingyunshan Cu-Au deposit in the Dehua-Youxi area of Fujian Province, southeastern China: Constraints from U-Pb and Re-Os geochronology, fluid inclusions, and H-O-S-Pb isotope data. Ore Geology Reviews, 2021, 132, 104006.	2.7	11
34	New identification and significance of Early Cretaceous mafic rocks in the interior South China Block. Scientific Reports, 2021, 11, 11396.	3.3	4
35	Factors controlling the formation of large porphyry Cu deposits: A case study from the Jiurui ore district of Middle-Lower Yangtze River Metallogenic Belt using in situ zircon and apatite chemistry from syn-mineralization intrusions. Ore Geology Reviews, 2021, 133, 104082.	2.7	12
36	Multiple generations of tourmaline from Yushishanxi leucogranite in South Qilian of western China record a complex formation history from B-rich melt to hydrothermal fluid. American Mineralogist, 2021, 106, 994-1008.	1.9	9

#	Article	IF	CITATIONS
37	Mineral Resource Science in China: Review and perspective. Geography and Sustainability, 2021, 2, 107-114.	4.3	17
38	Fluid Inclusions and H-O-C-S-Pb Isotope Studies of the Xinmin Cu-Au-Ag Polymetallic Deposit in the Qinzhou-Hangzhou Metallogenic Belt, South China: Constraints on Fluid Origin and Evolution. Geofluids, 2021, 2021, 1-17.	0.7	0
39	Late Jurassic–Early Cretaceous irregular slab rollback of paleo-Pacific plate beneath southeastern China: Insights from the petrogenesis of volcanic rocks of Moshishan Group in Dazhou volcanic basin, Gan-Hang Belt. Lithos, 2021, 392-393, 106137.	1.4	3
40	Erosion and sedimentation in SE Tibet and Myanmar during the evolution of the Burmese continental margin from the Late Cretaceous to Early Neogene. Gondwana Research, 2021, 95, 149-175.	6.0	7
41	Competition of equilibrium and kinetic silicon isotope fractionation during silica precipitation from acidic to alkaline pH solutions in geothermal systems. Geochimica Et Cosmochimica Acta, 2021, 306, 44-62.	3.9	6
42	Geochemistry, zircon U–Pb geochronology, and Hf isotopes of the metavolcanic rocks in the Tongbai orogen of central China: Implication for Neoproterozoic oceanic subduction to slab break-off. Precambrian Research, 2021, 361, 106239.	2.7	4
43	Two episodic Au–Mo mineralization in the Laowan district from the Tongbai orogenic belt of China: Constraints from U–Pb dating of zircon, rutile, and REE phosphate, and Re–Os dating of molybdenite. Gondwana Research, 2021, 96, 142-162.	6.0	11
44	Hydrothermal titanite U–Pb age and geochemistry as a reliable chronometer and genetic tracer for quartz vein-type tungsten deposit at Qipangou of Qinling orogenic belt, Central China. Ore Geology Reviews, 2021, 135, 104246.	2.7	6
45	Chlorine isotope fractionation during serpentinization and hydrothermal mineralization: A density functional theory study. Chemical Geology, 2021, 581, 120406.	3.3	6
46	Chlorine and sulfur evolution in magmatic rocks: A record from amphibole and apatite in the Tonglvshan Cu-Fe (Au) skarn deposit in Hubei Province, south China. Ore Geology Reviews, 2021, 137, 104312.	2.7	5
47	Apatite texture and trace element chemistry of carbonatite-related REE deposits in China: Implications for petrogenesis. Lithos, 2021, 398-399, 106276.	1.4	14
48	Zircon Hf O isotope and magma oxidation state evidence for the origin of Early Cretaceous granitoids and porphyry Mo mineralization in the Tongbai-Hong'an-Dabie orogens, Eastern China. Lithos, 2021, 398-399, 106281.	1.4	5
49	Late Triassic post-collisional high-K two-mica granites in Peninsular Thailand, SE Asia: Petrogenesis and Sn mineralization potential. Lithos, 2021, 398-399, 106290.	1.4	3
50	Indosinian magmatic–hydrothermal metallogenic event in the North Wuyi area, southeastern China: An example from the Chenfang skarn deposit in Jiangxi Province. Ore Geology Reviews, 2021, 138, 104386.	2.7	1
51	Magmatic-Hydrothermal Mineralization Processes at the Yidong Tin Deposit, South China: Insights from In Situ Chemical and Boron Isotope Changes of Tourmaline. Economic Geology, 2021, 116, 1625-1647.	3.8	21
52	Fluid origin and evolution of the Ruanjiawan W-Cu-(Mo) deposit from the Edong District in the Middle-Lower Yangtze River metallogenic belt of China: Constraints from fluid inclusions and H-O-C-S isotopes. Ore Geology Reviews, 2021, 139, 104428.	2.7	5
53	Complex REE systematics of carbonatites and weathering products from uniquely rich Mount Weld REE deposit, Western Australia. Ore Geology Reviews, 2021, 139, 104539.	2.7	18
54	Rare-metal mineralization potential and petrogenesis of Early Cretaceous I-type granitic rocks in the Lizikeng volcanic basin of Jiangxi Province, South China: evidence from mineralogy, geochemistry, and geochronology. Mineralium Deposita, 2020, 55, 453-468.	4.1	6

#	Article	IF	CITATIONS
55	Improved in-situ Determination of Sr Isotope Ratio in Silicate Samples Using LA-MC-ICP-MS and Its Wider Application for Fused Rock Powder. Journal of Earth Science (Wuhan, China), 2020, 31, 262-270.	3.2	5
56	Fluid inclusions and H–O–C–S isotope constraints on fluid evolution and ore genesis of the Wangjiadashan Cu–Au deposit in Suizao area of the Tongbaiâ€Đabie orogenic belt, central China. Geological Journal, 2020, 55, 1563-1586.	1.3	4
57	The formation of the ore-bearing dolomite marble from the giant Bayan Obo REE-Nb-Fe deposit, Inner Mongolia: insights from micron-scale geochemical data. Mineralium Deposita, 2020, 55, 131-146.	4.1	43
58	Tourmaline as a recorder of contrasting boron source and potential tin mineralization in the Mopanshan pluton from Inner Mongolia, northeastern China. Lithos, 2020, 354-355, 105284.	1.4	11
59	Petrogenesis of the Late Mesozoic Qijinfeng Granite Complex in the Tongbai orogen: Geochronological, geochemical and Sr-Nd-Pb-Hf isotope evidence. Lithos, 2020, 356-357, 105290.	1.4	10
60	Accurate Determination of Barium Isotopic Compositions in Sequentially Leached Phases from Carbonates by Double Spike-Thermal Ionization Mass Spectrometry (DS-TIMS). Analytical Chemistry, 2020, 92, 2417-2424.	6.5	12
61	Distal relationship of the Taihexian Pb-Zn-(Au) deposit to the Dengfuxian magmatic-hydrothermal system, South China: Constraints from mineralogy, fluid inclusion, H-O-Pb and in situ S isotopes. Ore Geology Reviews, 2020, 127, 103826.	2.7	7
62	Geochronology, mineral chemistry and genesis of REE mineralization in alkaline rocks from the Kohistan Island Arc, Pakistan. Ore Geology Reviews, 2020, 126, 103749.	2.7	7
63	Cretaceous granitic magmatism and mineralization in the Shanhu W-Sn ore deposit in the Nanling Range in South China. Ore Geology Reviews, 2020, 126, 103758.	2.7	14
64	The effect of magma differentiation and degassing on ore metal enrichment during the formation of the world-class Zhuxi W-Cu skarn deposit: Evidence from U-Pb ages, Hf isotopes and trace elements of zircon, and whole-rock geochemistry. Ore Geology Reviews, 2020, 127, 103801.	2.7	20
65	Boron isotope variations in tourmaline from hydrothermal ore deposits: A review of controlling factors and insights for mineralizing systems. Ore Geology Reviews, 2020, 125, 103682.	2.7	44
66	Constraints on the Petrogenesis and Metallogenic Setting of Lamprophyres in the World-Class Zhuxi W–Cu Skarn Deposit, South China. Minerals (Basel, Switzerland), 2020, 10, 642.	2.0	11
67	Spatialâ€Temporal Distribution, Geological Characteristics and Oreâ€Formation Controlling Factors of Major Types of Rare Metal Mineral Deposits in China. Acta Geologica Sinica, 2020, 94, 1757-1773.	1.4	16
68	Significance of hydrothermal reworking for REE mineralization associated with carbonatite: Constraints from in situ trace element and C-Sr isotope study of calcite and apatite from the Miaoya carbonatite complex (China). Geochimica Et Cosmochimica Acta, 2020, 280, 340-359.	3.9	48
69	Origin of paleosubduction-modified mantle for Late Cretaceous (~100ÂMa) diabase in northern Guangdong, South China: Geochronological and geochemical evidence. Lithos, 2020, 370-371, 105603.	1.4	4
70	Hydrothermally induced 34S enrichment in pyrite as an alternative explanation of the Late-Devonian sulfur isotope excursion in South China. Geochimica Et Cosmochimica Acta, 2020, 283, 1-21.	3.9	22
71	Fluid Evolution and Scheelite Precipitation Mechanism of the Large-Scale Shangfang Quartz-Vein-Type Tungsten Deposit, South China: Constraints from Rare Earth Element (REE) Behaviour during Fluid/Rock Interaction. Journal of Earth Science (Wuhan, China), 2020, 31, 635-652.	3.2	11
72	Granite–pegmatite connection and mineralization age of the giant Renli Ta Nb deposit in South China: Constraints from U–Th–Pb geochronology of coltan, monazite, and zircon. Lithos, 2020, 358-359, 105422.	1.4	16

#	Article	IF	CITATIONS
73	New constraints on the onset age of the Emeishan LIP volcanism and implications for the Guadalupian mass extinction. Lithos, 2020, 360-361, 105441.	1.4	10
74	Sr and Nd isotopes of cold seep carbonates from the northern South China sea as proxies for fluid sources. Marine and Petroleum Geology, 2020, 115, 104284.	3.3	8
75	Trace Metal and Cd Isotope Systematics of the Basal Datangpo Formation, Yangtze Platform (South) Tj ETQq1 1 (Switzerland), 2020, 10, 36.	0.784314 2.2	rgBT /Over 16
76	Exploration of driving mechanisms of equilibrium boron isotope fractionation in tourmaline group minerals and fluid: A density functional theory study. Chemical Geology, 2020, 536, 119466.	3.3	20
77	Origin and evolution of uraniferous pegmatite: A case study from the Xiaohuacha granite–pegmatite system and related country rocks in the Shangdan uranium mineralization district of North Qinling Orogenic Belt, China. Lithos, 2020, 356-357, 105379.	1.4	4
78	Discrete Jurassic and Cretaceous Mineralization Events at the Xiangdong W(-Sn) Deposit, Nanling Range, South China. Economic Geology, 2020, 115, 385-413.	3.8	57
79	In-situ elemental and boron isotopic variations of tourmaline from the Maogongdong deposit in the Dahutang W-Cu ore field of northern Jiangxi Province, South China: Insights into magmatic-hydrothermal evolution. Ore Geology Reviews, 2020, 122, 103502.	2.7	13
80	Evolution of the carbonatite Mo-HREE deposits in the Lesser Qinling Orogen: Insights from in situ geochemical investigation of calcite and sulfate. Ore Geology Reviews, 2019, 113, 103069.	2.7	24
81	Ore genesis of Kongxigou and Nanmushu Zn-Pb deposits hosted in Neoproterozoic carbonates, Yangtze Block, SW China: Constraints from sulfide chemistry, fluid inclusions, and in situ S-Pb isotope analyses. Precambrian Research, 2019, 333, 105405.	2.7	13
82	An effective method to distinguish between artificial and authigenic gypsum in marine sediments. Marine and Petroleum Geology, 2019, 110, 706-716.	3.3	3
83	Geological characteristics, fluid inclusions and H-O-C-S isotopes of the Zaopa Ag-Mo prospect in the Suizao area, Hubei Province: Implications for ore genesis. Ore Geology Reviews, 2019, 111, 103012.	2.7	8
84	Fluid inclusion and isotopic (C, H, O, S and Pb) constraints on the origin of late Mesozoic vein-type W mineralization in northern Guangdong, South China. Ore Geology Reviews, 2019, 112, 103007.	2.7	17
85	Cd isotopes trace periodic (bio)geochemical metal cycling at the verge of the Cambrian animal evolution. Geochimica Et Cosmochimica Acta, 2019, 263, 195-214.	3.9	27
86	The origin of rare alkali metals in geothermal fluids of southern Tibet, China: A silicon isotope perspective. Scientific Reports, 2019, 9, 7918.	3.3	12
87	Survived Seamount Reveals an in situ Origin for the Central Qiangtang Metamorphic Belt in the Tibetan Plateau. Journal of Earth Science (Wuhan, China), 2019, 30, 1253-1265.	3.2	4
88	Timing and Source of the Hermyingyi W-Sn Deposit in Southern Myanmar, SE Asia: Evidence from Molybdenite Re-Os Age and Sulfur Isotopic Composition. Journal of Earth Science (Wuhan, China), 2019, 30, 70-79.	3.2	14
89	Stable isotopes and rare earth element compositions of ancient cold seep carbonates from Enza River, northern Apennines (Italy): Implications for fluids sources and carbonate chimney growth. Marine and Petroleum Geology, 2019, 109, 434-448.	3.3	12
90	Petrogenesis and tectonic implications of Early Cretaceous shoshonitic syenites in the northern Wuyi Mt Range, Southeast China. Journal of Asian Earth Sciences, 2019, 180, 103877.	2.3	8

#	Article	IF	CITATIONS
91	Fluid Inclusions and H-O-C-S Isotopes of the Wushan Copper Polymetallic Deposit in the Suizao Area, Hubei Province: Implications for Ore Genesis. Geofluids, 2019, 2019, 1-29.	0.7	4
92	Silicon Isotope Geochemistry: Fractionation Linked to Silicon Complexations and Its Geological Applications. Molecules, 2019, 24, 1415.	3.8	12
93	Effect of Beam Current and Diameter on Electron Probe Microanalysis of Carbonate Minerals. Journal of Earth Science (Wuhan, China), 2019, 30, 834-842.	3.2	12
94	In situ major and trace element analysis of magnetite from carbonatite-related complexes: Implications for petrogenesis and ore genesis. Ore Geology Reviews, 2019, 107, 30-40.	2.7	23
95	Origin of the Shangfang Tungsten Deposit in the Fujian Province of Southeast China: Evidence from Scheelite Sm–Nd Geochronology, H–O Isotopes and Fluid Inclusions Studies. Minerals (Basel,) Tj ETQq1 1 0	.78 4.3 14 rg	gBT6/Overlock
96	Elemental and B-O-H isotopic compositions of tourmaline and associated minerals in biotite-muscovite granite of Mashhad, NE Iran: Constraints on tourmaline genesis and element partitioning. Lithos, 2019, 324-325, 803-820.	1.4	13
97	Hydrothermal evolution and ore genesis of the Zhaiping Ag-Pb-Zn deposit in Fujian Province of Southeast China: Evidence from stable isotopes (H, O, C, S) and fluid inclusions. Ore Geology Reviews, 2019, 104, 246-265.	2.7	16
98	In-situ elemental and boron isotopic variations of tourmaline from the Sanfang granite, South China: Insights into magmatic-hydrothermal evolution. Chemical Geology, 2019, 504, 190-204.	3.3	44
99	Gold distribution and source of the J4 gold-bearing breccia pipe in the Qiyugou district, North China Craton: Constraints from ore mineralogy and in situ analysis of trace elements and S-Pb isotopes. Ore Geology Reviews, 2019, 105, 514-536.	2.7	25
100	Positive cerium anomaly in the Doushantuo cap carbonates from the Yangtze platform, South China: Implications for intermediate water column manganous conditions in the aftermath of the Marinoan glaciation. Precambrian Research, 2019, 320, 93-110.	2.7	19
101	Detrital zircons in metasedimentary rocks of Mayuan and Mamianshan Group from Cathaysia Block in northwestern Fujian Province, South China: New constraints on their formation ages and paleogeographic implication. Precambrian Research, 2019, 320, 13-30.	2.7	29
102	Petrogenesis and Tectonic Implications of the Yuhuashan A-Type Volcanic-Intrusive Complex and Mafic Microgranular Enclaves in the Gan-Hang Volcanic Belt, Southeast China. Journal of Geology, 2019, 127, 37-59.	1.4	6
103	Basaltic and Solution Reference Materials for Iron, Copper and Zinc Isotope Measurements. Geostandards and Geoanalytical Research, 2019, 43, 163-175.	3.1	29
104	Trace Elements Characteristics of Black Shales from the Ediacaran Doushantuo Formation, Hubei Province, South China: Implications for Redox and Open vs. Restricted Basin Conditions. Journal of Earth Science (Wuhan, China), 2018, 29, 342-352.	3.2	16
105	In situ Analysis of Major Elements, Trace Elements and Sr Isotopic Compositions of Apatite from the Granite in the Chengchao Skarn-Type Fe Deposit, Edong Ore District: Implications for Petrogenesis and Mineralization. Journal of Earth Science (Wuhan, China), 2018, 29, 295-306.	3.2	22
106	Fluid inclusion and O–H–C isotopic constraints on the origin and evolution of ore-forming fluids of the Cenozoic volcanic-hosted Kuh-Pang copper deposit, Central Iran. Ore Geology Reviews, 2018, 94, 277-289.	2.7	13
107	Fluid evolution and ore genesis of the Dalingshang deposit, Dahutang W-Cu ore field, northern Jiangxi Province, South China. Mineralium Deposita, 2018, 53, 1079-1094.	4.1	26
108	U-Pb Ages and Lu-Hf Isotopes of Detrital Zircons from Sedimentary Units across the Mid-Neoproterozoic Unconformity in the Western Jiangnan Orogen of South China and Their Tectonic Implications. Journal of Geology, 2018, 126, 207-228.	1.4	13

#	Article	IF	CITATIONS
109	Using apatite to discriminate synchronous ore-associated and barren granitoid rocks: A case study from the Edong metallogenic district, South China. Lithos, 2018, 310-311, 369-380.	1.4	35
110	Early Jurassic mafic dykes from the Aigao uranium ore deposit in South China: Geochronology, petrogenesis and relationship with uranium mineralization. Lithos, 2018, 308-309, 118-133.	1.4	22
111	Ore genesis of the Wusihe carbonate-hosted Zn-Pb deposit in the Dadu River Valley district, Yangtze Block, SW China: evidence from ore geology, S-Pb isotopes, and sphalerite Rb-Sr dating. Mineralium Deposita, 2018, 53, 967-979.	4.1	38
112	Diverse lamprophyres origins corresponding to lithospheric thinning: a case study in the Jiurui district of Middle-Lower Yangtze River Belt, South China Craton. Gondwana Research, 2018, 54, 62-80.	6.0	14
113	Iron isotope behavior during fluid/rock interaction in K-feldspar alteration zone – A model for pyrite in gold deposits from the Jiaodong Peninsula, East China. Geochimica Et Cosmochimica Acta, 2018, 222, 94-116.	3.9	50
114	Oxygen fugacity, temperature and pressure estimation from mineral chemistry of the granodiorite porphyry from the Jilongshan Au-Cu deposit and the Baiguoshu prospecting area in SE Hubei Province: A guide for mineral exploration. Journal of Geochemical Exploration, 2018, 184, 136-149.	3.2	4
115	Petrogenesis of Cretaceous volcanic-intrusive complex from the giant Yanbei tin deposit, South China: Implication for multiple magma sources, tin mineralization, and geodynamic setting. Lithos, 2018, 296-299, 163-180.	1.4	31
116	Isotope geochemistry and genesis of the Liyuan gold deposit, Shanxi, North China. Ore Geology Reviews, 2018, 92, 129-143.	2.7	10
117	Fluid Evolution of Fuzishan Skarn Cu-Mo Deposit from the Edong District in the Middle-Lower Yangtze River Metallogenic Belt of China: Evidence from Petrography, Mineral Assemblages, and Fluid Inclusions. Geofluids, 2018, 2018, 1-25.	0.7	0
118	Major, trace and rare earth elements of apatite and zircon U-Pb ages of ore-associated and barren granitoids from the Edong ore district, South China. Data in Brief, 2018, 20, 1587-1601.	1.0	1
119	Mechanism of boron incorporation into calcites and associated isotope fractionation in a steady-state carbonate-seawater system. Applied Geochemistry, 2018, 98, 221-236.	3.0	13
120	Ore-forming fluids and isotopic (H-O-C-S-Pb) characteristics of the Fujiashan-Longjiaoshan skarn W-Cu-(Mo) deposit in the Edong District of Hubei Province, China. Ore Geology Reviews, 2018, 102, 386-405.	2.7	19
121	In-situ sulfur isotope and trace element analysis of pyrite from the Xiwang uranium ore deposit in South China: Implication for ore genesis. Journal of Geochemical Exploration, 2018, 195, 49-65.	3.2	22
122	Radiogenic Pb reservoir contributes to the rare earth element (REE) enrichment in South Qinling carbonatites. Chemical Geology, 2018, 494, 80-95.	3.3	32
123	Highly fractionated Jurassic I-type granites and related tungsten mineralization in the Shirenzhang deposit, northern Guangdong, South China: Evidence from cassiterite and zircon U-Pb ages, geochemistry and Sr-Nd-Pb-Hf isotopes. Lithos, 2018, 312-313, 186-203.	1.4	72
124	Origin of the granites and related Sn and Pb-Zn polymetallic ore deposits in the Pengshan district, Jiangxi Province, South China: constraints from geochronology, geochemistry, mineral chemistry, and Sr-Nd-Hf-Pb-S isotopes. Mineralium Deposita, 2017, 52, 337-360.	4.1	36
125	Genesis of the giant Zijinshan epithermal Cu-Au and Luoboling porphyry Cu–Mo deposits in the Zijinshan ore district, Fujian Province, SE China: A multi-isotope and trace element investigation. Ore Geology Reviews, 2017, 88, 753-767.	2.7	31
126	Sulfide chemistry and sulfur isotope characteristics of the Cenozoic volcanic-hosted Kuh-Pang copper deposit, Saveh county, northwestern central Iran. Ore Geology Reviews, 2017, 86, 563-583.	2.7	25

#	Article	IF	CITATIONS
127	In situ major and trace element analysis of amphiboles in quartz monzodiorite porphyry from the Tonglvshan Cu–Fe (Au) deposit, Hubei Province, China: insights into magma evolution and related mineralization. Contributions To Mineralogy and Petrology, 2017, 172, 1.	3.1	21
128	Transient deep-water oxygenation in the early Cambrian Nanhua Basin, South China. Geochimica Et Cosmochimica Acta, 2017, 210, 42-58.	3.9	70
129	Geochemistry of Ediacaran cap dolostones across the Yangtze Platform, South China: implications for diagenetic modification and seawater chemistry in the aftermath of the Marinoan glaciation. Journal of the Geological Society, 2017, 174, 893-912.	2.1	17
130	Petrogenesis and geodynamic setting of Early Cretaceous felsic rocks in the Gan-Hang Belt, Southeast China: Constraints from geochronology and geochemistry of the tuffs and trachyandesitic rocks in Shengyuan volcanic Basin. Lithos, 2017, 284-285, 691-708.	1.4	17
131	The Mafic–Ultramafic Dykes in the Yanbian Terrane (Sichuan Province, SW China): Record of Magma Differentiation and Emplacement in the Emeishan Large Igneous Province. Journal of Petrology, 2017, 58, 513-538.	2.8	11
132	A LA-ICP-MS analysis of rare earth elements on phosphatic grains of the Ediacaran Doushantuo phosphorite at Weng'an, South China: implication for depositional conditions and diagenetic processes. Geological Magazine, 2017, 154, 1381-1397.	1.5	28
133	Sulfur isotope fractionation in pyrite during laser ablation: Implications for laser ablation multiple collector inductively coupled plasma mass spectrometry mapping. Chemical Geology, 2017, 450, 223-234.	3.3	77
134	Occurrence, source and enrichment mechanism of silver in black shale-hosted Baiguoyuan Ag-V ore deposit, Hubei Province, China. Journal of Geochemical Exploration, 2017, 183, 79-87.	3.2	5
135	Production, consumption, and migration of methane in accretionary prism of southwestern Taiwan. Geochemistry, Geophysics, Geosystems, 2017, 18, 2970-2989.	2.5	28
136	A comparison study of tungsten-bearing granite and related mineralization in the northern Jiangxi-southern Anhui provinces and southern Jiangxi Province in South China. Science China Earth Sciences, 2017, 60, 1942-1958.	5.2	34
137	Partial Melting of Subducted Sediments Produced Early Mesozoic Calc-alkaline Lamprophyres from Northern Guangxi Province, South China. Scientific Reports, 2017, 7, 4864.	3.3	19
138	In situ U–Th–Pb ages of the Miaoya carbonatite complex in the South Qinling orogenic belt, central China. Lithos, 2017, 290-291, 159-171.	1.4	54
139	Inâ€situ analysis of trace elements and Sr–Pb isotopes of Kâ€feldspars from Tongshankou Cu–Mo deposit, SE Hubei Province, China: Insights into early potassic alteration of the porphyry mineralization system. Terra Nova, 2017, 29, 343-355.	2.1	8
140	Matrix Effects Originating from Coexisting Minerals and Accurate Determination of Stable Silver Isotopes in Silver Deposits. Analytical Chemistry, 2017, 89, 13634-13641.	6.5	9
141	In Situ Carbon Isotope Analysis by Laser Ablation MC-ICP-MS. Analytical Chemistry, 2017, 89, 13415-13421.	6.5	15
142	Br/Cl, I/Cl and chlorine isotopic compositions of pore water in shallow sediments: implications for the fluid sources in the Dongsha area, northern South China Sea. Acta Oceanologica Sinica, 2017, 36, 31-36.	1.0	15
143	Geochronological, geochemical and Sr-Nd-Hf isotopic constraints on the petrogenesis of Late Cretaceous A-type granites from the Sibumasu Block, Southern Myanmar, SE Asia. Lithos, 2017, 268-271, 32-47.	1.4	58
144	The geochemistry, U-Pb and Re-Os geochronology, and Hf isotopic constraints on the genesis of the Huangjiagou Mo deposit and related granite in the Dabie region, Hubei Province, China. Ore Geology Reviews, 2017, 81, 504-517.	2.7	20

#	Article	IF	CITATIONS
145	Geochemistry of Monazite within Carbonatite Related REE Deposits. Resources, 2017, 6, 51.	3.5	40
146	Origin and Evolution of the Ore-Forming Fluids in the Liyuan Gold Deposit, Central North China Craton: Constraints from Fluid Inclusions and H-O-C Isotopic Compositions. Geofluids, 2017, 2017, 1-21.	0.7	10
147	Genesis of the Zhijiadi Ag-Pb-Zn Deposit, Central North China Craton: Constraints from Fluid Inclusions and Stable Isotope Data. Geofluids, 2017, 2017, 1-23.	0.7	9
148	Nature and Evolution of the Ore-Forming Fluids from Nanmushu Carbonate-Hosted Zn-Pb Deposit in the Mayuan District, Shaanxi Province, Southwest China. Geofluids, 2017, 2017, 1-19.	0.7	13
149	A Preliminary Identification of Micro/Nano Scale Textures on Mineralization, Hydrocarbon Accumulation and Seismic Formation Structure. Journal of Nanoscience and Nanotechnology, 2017, 17, 7048-7054.	0.9	2
150	Studies on Micro/Nano-Sized Grinding Grains on Shear-Slip Surfaces in Rocks. Journal of Nanoscience and Nanotechnology, 2017, 17, 7069-7075.	0.9	1
151	Mapping of Sulfur Isotopes and Trace Elements in Sulfides by LA-(MC)-ICP-MS: Potential Analytical Problems, Improvements and Implications. Minerals (Basel, Switzerland), 2016, 6, 110.	2.0	68
152	A Possible Mechanism to Thin Lithosphere of the North China Craton: Insights from Cretaceous Mafic Dikes in the Jiaodong Pensinsula. Acta Geologica Sinica, 2016, 90, 106-108.	1.4	1
153	Pore water geochemistry in shallow sediments from the northeastern continental slope of the South China sea. Marine and Petroleum Geology, 2016, 75, 68-82.	3.3	28
154	Rare earth element geochemistry of phosphatic rocks in Neoproterozoic Ediacaran Doushantuo Formation in Hushan Section from the Yangtze Gorges Area, South China. Journal of Earth Science (Wuhan, China), 2016, 27, 204-210.	3.2	30
155	Marine Mo biogeochemistry in the context of dynamically euxinic mid-depth waters: A case study of the lower Cambrian Niutitang shales, South China. Geochimica Et Cosmochimica Acta, 2016, 183, 79-93.	3.9	90
156	Rapid lithospheric thinning of the North China Craton: New evidence from cretaceous mafic dikes in the Jiaodong Peninsula. Chemical Geology, 2016, 432, 1-15.	3.3	96
157	Matrix effects of calcium on high-precision sulfur isotope measurement by multiple-collector inductively coupled plasma mass spectrometry. Talanta, 2016, 151, 132-140.	5.5	11
158	Zircon U–Pb dating, geochemical and Sr–Nd–Hf isotopic characteristics of the Jintonghu monzonitic rocks in western Fujian Province, South China: Implication for Cretaceous crust–mantle interactions and lithospheric extension. Lithos, 2016, 260, 413-428.	1.4	30
159	A petrographic and geochemical study of carbonate and silica phases from the Ediacaran Doushantuo Formation in the Three Gorges area of South China: Implications for diagenetic conditions. Palaeogeography, Palaeoclimatology, Palaeoecology, 2016, 463, 150-167.	2.3	14
160	Petrogenesis of Late Jurassic granodiorites from Gutian, Fujian Province, South China: Implications for multiple magma sources and origin of porphyry Cu–Mo mineralization. Lithos, 2016, 264, 540-554.	1.4	31
161	Sr isotopic compositions of the interstitial water and carbonate from two basins in the Gulf of Mexico: Implications for fluid flow and origin. Chemical Geology, 2016, 439, 43-51.	3.3	5
162	Trace and rare earth element characteristics in Fe-Mn carbonates associated with stratiform Ag-Pb-Zn mineralization from the Lengshuikeng ore district, Jiangxi Province: Implications for their genesis and depositional environment. Journal of Earth Science (Wuhan, China), 2016, 27, 571-583.	3.2	13

#	Article	IF	CITATIONS
163	Adsorption Behavior of Metasilicate on N-Methyl d-Glucamine Functional Groups and Associated Silicon Isotope Fractionation. Langmuir, 2016, 32, 8872-8881.	3.5	8
164	Geochronology and geochemical constraints on petrogenesis of Early Paleozoic granites from the Laojunshan district in Yunnan Province of South China. Gondwana Research, 2016, 29, 248-263.	6.0	21
165	Geochemistry, geochronology and Sr–Nd–Pb–Hf isotopic compositions of Middle to Late Jurassic syenite–granodiorites–dacite in South China: Petrogenesis and tectonic implications. Gondwana Research, 2016, 35, 217-237.	6.0	31
166	Rapid determination of boron isotopic composition (l̂´ ¹¹ B) in pore water by multi-collector inductively coupled plasma mass spectrometry. Analytical Methods, 2016, 8, 1721-1727.	2.7	3
167	Late Triassic U-bearing and barren granites in the Miao'ershan batholith, South China: Petrogenetic discrimination and exploration significance. Ore Geology Reviews, 2016, 77, 260-278.	2.7	37
168	U–Pb dating of zircons from tuff layer, sandstone and tillite samples in the uppermost Liantuo Formation and the lowermost Nantuo Formation in Three Gorges area, South China. Chemie Der Erde, 2016, 76, 103-109.	2.0	13
169	Geochronology, geochemistry and tectonic significance of the late Mesozoic volcanic sequences in the northern Wuyi Mountain volcanic belt of South China. Gondwana Research, 2016, 37, 362-383.	6.0	20
170	An object-oriented diagnostic model for the quantification of porewater geochemistry in marine sediments. Journal of Earth Science (Wuhan, China), 2015, 26, 648-660.	3.2	1
171	Improvements on high-precision measurement of bromine isotope ratios by multicollector inductively coupled plasma mass spectrometry. Talanta, 2015, 143, 302-306.	5.5	8
172	Rise to modern levels of ocean oxygenation coincided with the Cambrian radiation of animals. Nature Communications, 2015, 6, 7142.	12.8	250
173	Geochronology and Hf isotope study of pegmatite in the Xiaoqinling area of NW China: Implication for petrogenesis and regional metamorphism. Journal of Earth Science (Wuhan, China), 2015, 26, 295-305.	3.2	20
174	Tourmaline as a recorder of magmatic–hydrothermal evolution: an in situ major and trace element analysis of tourmaline from the Qitianling batholith, South China. Contributions To Mineralogy and Petrology, 2015, 170, 1.	3.1	57
175	Improvements in Cu–Zn isotope analysis with MC-ICP-MS: A revisit of chemical purification, mass spectrometry measurement and mechanism of Cu/Zn mass bias decoupling effect. International Journal of Mass Spectrometry, 2015, 393, 34-40.	1.5	15
176	Late Cretaceous granites from the giant Dulong Sn-polymetallic ore district in Yunnan Province, South China: Geochronology, geochemistry, mineral chemistry and Nd–Hf isotopic compositions. Lithos, 2015, 218-219, 54-72.	1.4	104
177	Mineral chemistry and H–O–S–Pb isotopic compositions of skarn type copper deposits in the Jiurui district of the Middle-Lower Yangtze River metallogenic belt, Eastern China. Ore Geology Reviews, 2015, 69, 88-103.	2.7	18
178	Lipid biomarkers and their specific carbon isotopic compositions ofÂcold seep carbonates from the South China Sea. Marine and Petroleum Geology, 2015, 66, 501-510.	3.3	20
179	Rare earth element and Sr–Nd isotope geochemistry of phosphatic rocks in Neoproterozoic Ediacaran Doushantuo Formation in Zhangcunping section from western Hubei Province, South China. Palaeogeography, Palaeoclimatology, Palaeoecology, 2015, 440, 712-724.	2.3	27
180	Secular changes of water chemistry in shallow-water Ediacaran ocean: Evidence from carbonates at Xiaofenghe, Three Gorges area, Yangtze Platform, South China. Precambrian Research, 2015, 270, 50-79.	2.7	25

#	Article	IF	CITATIONS
181	Chemical and boron isotopic compositions of tourmaline from the Nyalam leucogranites, South Tibetan Himalaya: Implication for their formation from B-rich melt to hydrothermal fluids. Chemical Geology, 2015, 419, 102-113.	3.3	54
182	Cretaceous crust–mantle interaction and tectonic evolution of Cathaysia Block in South China: Evidence from pulsed mafic rocks and related magmatism. Tectonophysics, 2015, 661, 136-155.	2.2	29
183	High precision in-situ Pb isotopic analysis of sulfide minerals by femtosecond laser ablation multi-collector inductively coupled plasma mass spectrometry. Science China Earth Sciences, 2015, 58, 1713-1721.	5.2	56
184	Implication of Boron Isotope Geochemistry for the Pedogenic Environments in Loess and Paleosol Sequences of Central China. Quaternary Research, 2015, 83, 243-255.	1.7	10
185	A subduction-related metasomatically enriched mantle origin for the Luoboling and Zhongliao Cretaceous granitoids from South China: implications for magma evolution and Cu–Mo mineralization. International Geology Review, 2015, 57, 1239-1266.	2.1	36
186	Geology and fluid characteristics of the Ulu Sokor gold deposit, Kelantan, Malaysia: Implications for ore genesis and classification of the deposit. Ore Geology Reviews, 2015, 64, 400-424.	2.7	13
187	Rapid and high-precision measurement of sulfur isotope and sulfur concentration in sediment pore water by multi-collector inductively coupled plasma mass spectrometry. Talanta, 2015, 132, 8-14.	5.5	6
188	Zircon U–Pb geochronology, geochemical and Sr–Nd–Hf isotopic compositions of the Triassic granite and diorite dikes from the Wulonggou mining area in the Eastern Kunlun Orogen, NW China: Petrogenesis and tectonic implications. Lithos, 2014, 205, 266-283.	1.4	107
189	Reliability of LA-ICP-MS U-Pb dating of zircons with high U concentrations: A case study from the U-bearing Douzhashan Granite in South China. Chemical Geology, 2014, 389, 110-121.	3.3	47
190	Geochronology, geochemistry, and mineralization of the granodiorite porphyry hosting the Matou Cu–Mo (±W) deposit, Lower Yangtze River metallogenic belt, eastern China. Journal of Asian Earth Sciences, 2014, 79, 623-640.	2.3	43
191	A rapid and highâ€precision method for sulfur isotope Î′ ³⁴ S determination with a multipleâ€collector inductively coupled plasma mass spectrometer: matrix effect correction and applications for water samples without chemical purification. Rapid Communications in Mass Spectrometry, 2014, 28, 750-756.	1.5	16
192	An improved procedure for separation/purification of boron from complex matrices and high-precision measurement of boron isotopes by positive thermal ionization and multicollector inductively coupled plasma mass spectrometry. Talanta, 2014, 123, 151-160.	5.5	24
193	Geology, geochemistry and ore genesis of the Wenyu gold deposit, Xiaoqinling gold field, Qinling Orogen, southern margin of North China Craton. Ore Geology Reviews, 2014, 59, 1-20.	2.7	95
194	Effect of metasilicate matrices on boron purification by Amberlite IRA 743 boron specific resin and isotope analysis by MC-ICP-MS. Journal of Analytical Atomic Spectrometry, 2014, 29, 2104-2107.	3.0	7
195	Geochronology and geochemistry of Cretaceous Nanshanping alkaline rocks from the Zijinshan district in Fujian Province, South China: Implications for crust–mantle interaction and lithospheric extension. Journal of Asian Earth Sciences, 2014, 93, 253-274.	2.3	32
196	Geochronology, elemental and Nd–Hf isotopic geochemistry of Devonian A-type granites in central Jiangxi, South China: Constraints on petrogenesis and post-collisional extension of the Wuyi–Yunkai orogeny. Lithos, 2014, 206-207, 1-18.	1.4	49
197	Petrogenesis of Late Mesozoic granitoids and coeval mafic rocks from the Jiurui district in the Middle–Lower Yangtze metallogenic belt of Eastern China: Geochemical and Sr–Nd–Pb–Hf isotopic evidence. Lithos, 2014, 190-191, 467-484.	1.4	38
198	Depositional environments for stratiform witherite deposits in the Lower Cambrian black shale sequence of the Yangtze Platform, southern Qinling region, SW China: Evidence from redox-sensitive trace element geochemistry. Palaeogeography, Palaeoclimatology, Palaeoecology, 2014, 398, 125-131.	2.3	68

#	Article	IF	CITATIONS
199	Boron isotope geochemistry of salt sediments from the Dongtai salt lake in Qaidam Basin: Boron budget and sources. Chemical Geology, 2014, 380, 74-83.	3.3	57
200	Rare earth element and SrNd isotope geochemistry of phosphate nodules from the lower Cambrian Niutitang Formation, NW Hunan Province, South China. Palaeogeography, Palaeoclimatology, Palaeoecology, 2014, 398, 132-143.	2.3	58
201	Mineralogy, geochemistry and ore genesis of the Dawan uranium deposit in southern Hunan Province, South China. Journal of Geochemical Exploration, 2014, 138, 59-71.	3.2	21
202	Lithospheric and asthenospheric sources of lamprophyres in the Jiaodong Peninsula: A consequence of rapid lithospheric thinning beneath the North China Craton?. Geochimica Et Cosmochimica Acta, 2014, 124, 250-271.	3.9	198
203	Boron isotopic fractionation and trace element incorporation in various species of modern corals in Sanya Bay, South China Sea. Journal of Earth Science (Wuhan, China), 2014, 25, 431-444.	3.2	7
204	Highly fractionated S-type granites from the giant Dahutang tungsten deposit in Jiangnan Orogen, Southeast China: geochronology, petrogenesis and their relationship with W-mineralization. Lithos, 2014, 202-203, 207-226.	1.4	180
205	Geochemistry of Early Cretaceous calc-alkaline lamprophyres in the Jiaodong Peninsula: Implication for lithospheric evolution of the eastern North China Craton. Gondwana Research, 2014, 25, 859-872.	6.0	135
206	Chronology, Hf isotopes, geochemistry, and petrogenesis of the magmatic rocks in the Shizishan ore field of Tongling, Anhui Province. Science China Earth Sciences, 2013, 56, 993-1013.	5.2	16
207	Geochemistry of pore waters from HQ-1PC of the Qiongdongnan Basin, northern South China Sea, and its implications for gas hydrate exploration. Science China Earth Sciences, 2013, 56, 521-529.	5.2	20
208	Major cation/chlorine ratio and stable chlorine isotopic compositions of sediment interstitial water in the Brazos-Trinity Basin IV from the Gulf of Mexico (IODP 308). Journal of Asian Earth Sciences, 2013, 65, 42-50.	2.3	7
209	Zircon U–Pb chronology and elemental and Sr–Nd–Hf isotope geochemistry of two Triassic A-type granites in South China: Implication for petrogenesis and Indosinian transtensional tectonism. Lithos, 2013, 160-161, 292-306.	1.4	88
210	Sr isotopic compositions of cold seep carbonates from the South China Sea and the Panoche Hills (California, USA) and their significance in palaeooceanography. Journal of Asian Earth Sciences, 2013, 65, 34-41.	2.3	18
211	Zircon U–Pb dating, trace element and Sr–Nd–Hf isotope geochemistry of Paleozoic granites in the Miao'ershan–Yuechengling batholith, South China: Implication for petrogenesis and tectonic–magmatic evolution. Journal of Asian Earth Sciences, 2013, 74, 244-264.	2.3	61
212	Re–Os geochronology of black shales from the Neoproterozoic Doushantuo Formation, Yangtze platform, South China. Precambrian Research, 2013, 225, 67-76.	2.7	78
213	Precise dating of the Middle Permian: Zircon U–Pb geochronology from volcanic ash beds in the basal Gufeng Formation, Yangtze region, South China. Gondwana Research, 2013, 23, 1599-1606.	6.0	22
214	Trace and rare earth element geochemistry of black shale and kerogen in the early Cambrian Niutitang Formation in Guizhou province, South China: Constraints for redox environments and origin of metal enrichments. Precambrian Research, 2013, 225, 218-229.	2.7	213
215	Origin of the Dachang gold deposit, NW China: constraints from H, O, S, and Pb isotope data. International Geology Review, 2013, 55, 1885-1901.	2.1	11
216	Petrogenesis and tectonic significance of Early Cretaceous high-Zr rhyolite in the Dazhou uranium district, Gan-Hang Belt, Southeast China. Journal of Asian Earth Sciences, 2013, 74, 303-315.	2.3	30

#	Article	IF	CITATIONS
217	Multiple sources for the origin of Late Jurassic Linglong adakitic granite in the Shandong Peninsula, eastern China: Zircon U–Pb geochronological, geochemical and Sr–Nd–Hf isotopic evidence. Lithos, 2013, 162-163, 251-263.	1.4	124
218	Occurrence and significance of a quartz–amphibole schist xenolith within a mafic microgranular enclave in the Xiangshan volcanic-intrusive complex, SE China. International Geology Review, 2013, 55, 894-903.	2.1	8
219	Precise Determination of the Absolute Isotopic Abundance Ratio and the Atomic Weight of Chlorine in Three International Reference Materials by the Positive Thermal Ionization Mass Spectrometer-Cs ₂ Cl ⁺ -Graphite Method. Analytical Chemistry, 2012, 84, 10350-10358.	6.5	23
220	An experimental study of organic matters that cause isobaric ions interference for boron isotopic measurement by thermal ionization mass spectrometry. International Journal of Mass Spectrometry, 2012, 328-329, 67-77.	1.5	7
221	Extraction and Determination of Boron Isotopic Composition in Tourmalines. Chinese Journal of Analytical Chemistry, 2012, 40, 1654-1660.	1.7	6
222	Geochemistry and petrogenesis of the Huashan granites and their implications for the Mesozoic tectonic settings in the Xiaoqinling gold mineralization belt, NW China. Journal of Asian Earth Sciences, 2012, 56, 276-289.	2.3	85
223	Geochemistry, geochronology and Sr–Nd–Hf isotopes of two Mesozoic granitoids in the Xiaoqinling gold district: Implication for large-scale lithospheric thinning in the North China Craton. Chemical Geology, 2012, 294-295, 173-189.	3.3	92
224	Chemical and boron isotopic composition of tourmaline in the Xiangshan volcanic–intrusive complex, Southeast China: Evidence for boron mobilization and infiltration during magmatic–hydrothermal processes. Chemical Geology, 2012, 312-313, 177-189.	3.3	47
225	Geochronology, geochemistry and tectonic significance of two Early Cretaceous A-type granites in the Gan-Hang Belt, Southeast China. Lithos, 2012, 150, 155-170.	1.4	132
226	Petrogenesis of the Middle Jurassic Yinshan volcanic-intrusive complex, SE China: Implications for tectonic evolution and Cu-Au mineralization. Lithos, 2012, 150, 135-154.	1.4	90
227	A new method to determine carbon isotopic composition of dissolved inorganic carbon in seawater and pore waters by CO ₂ â€water equilibrium. Rapid Communications in Mass Spectrometry, 2012, 26, 805-810.	1.5	4
228	Rare earth elements and carbon isotope geochemistry of the Doushantuo Formation in South China: Implication for middle Ediacaran shallow marine redox conditions. Science Bulletin, 2012, 57, 1998-2006.	1.7	34
229	Mineral chemistry, trace elements and Sr–Nd–Hf isotope geochemistry and petrogenesis of Cailing and Furong granites and mafic enclaves from the Qitianling batholith in the Shi-Hang zone, South China. Gondwana Research, 2012, 22, 310-324.	6.0	149
230	Zircon effect alone insufficient to generate seawater Ndâ€Hf isotope relationships. Geochemistry, Geophysics, Geosystems, 2011, 12, .	2.5	18
231	Uranium-bearing and barren granites from the Taoshan Complex, Jiangxi Province, South China: Geochemical and petrogenetic discrimination and exploration significance. Journal of Geochemical Exploration, 2011, 110, 126-135.	3.2	39
232	Crust recycling in the sources of two parallel volcanic chains in Shandong, North China. Earth and Planetary Science Letters, 2011, 302, 359-368.	4.4	106
233	Late Mesozoic magmatism of the Jiurui mineralization district in the Middle–Lower Yangtze River Metallogenic Belt, Eastern China: Precise U–Pb ages and geodynamic implications. Gondwana Research, 2011, 20, 831-843.	6.0	53
234	Geochemical, zircon U–Pb dating and Sr–Nd–Hf isotopic constraints on the age and petrogenesis of an Early Cretaceous volcanic-intrusive complex at Xiangshan, Southeast China. Mineralogy and Petrology, 2011, 101, 21-48.	1.1	89

#	Article	IF	CITATIONS
235	Glycerol ether biomarkers and their carbon isotopic compositions in a cold seep carbonate chimney from the Shenhu area, northern South China Sea. Science Bulletin, 2011, 56, 1700-1707.	1.7	22
236	Re-Os isotope dating of pyrite from the footwall mineralization zone of the Xinqiao deposit, Tongling, Anhui Province: Geochronological evidence for submarine exhalative sedimentation. Science Bulletin, 2011, 56, 3860-3865.	1.7	39
237	Trace-element, rare-earth element and boron isotopic compositions of tourmaline from a vein-type Pb–Zn–Cu±ÂU deposit, NE Turkey. International Geology Review, 2011, 53, 1-24.	2.1	30
238	Chemical environment of cold seep carbonate formation on the northern continental slope of South China Sea: Evidence from trace and rare earth element geochemistry. Marine Geology, 2010, 277, 21-30.	2.1	110
239	Subducting sediment-derived arc granitoids: evidence from the Datong pluton and its quenched enclaves in the western Kunlun orogen, northwest China. Mineralogy and Petrology, 2010, 100, 55-74.	1.1	31
240	Petrogenesis and tectonic implications of Late Jurassic shoshonitic lamprophyre dikes from the Liaodong Peninsula, NE China. Mineralogy and Petrology, 2010, 100, 127-151.	1.1	93
241	Zircon U-Pb geochronology, Hf isotopic composition and geological implications of the rhyodacite and rhyodacitic porphyry in the Xiangshan uranium ore field, Jiangxi Province, China. Science China Earth Sciences, 2010, 53, 1411-1426.	5.2	47
242	Geochemical characteristics of pore water in shallow sediments from Shenhu area of South China Sea and their significance for gas hydrate occurrence. Science Bulletin, 2010, 55, 752-760.	1.7	51
243	Hf isotopic composition of zircons from the Huashan-Guposhan intrusive complex and their mafic enclaves in northeastern Guangxi: Implication for petrogenesis. Science Bulletin, 2010, 55, 509-519.	1.7	41
244	Origin of ore-forming fluid in the Piaotang tungsten deposit in Jiangxi Province: Evidence from helium and argon isotopes. Science Bulletin, 2010, 55, 628-634.	1.7	31
245	A conduit-related genesis of the Lengshuiqing intrusive assemblage (Sichuan, SW China). Journal of Volcanology and Geothermal Research, 2010, 189, 118-130.	2.1	6
246	Boron concentration and isotopic constraints on processes affecting the chemistry of interstitial water in normal- and over-pressured basins, Gulf of Mexico. Marine Geology, 2010, 275, 230-243.	2.1	5
247	Carbonated mantle sources for Cenozoic intra-plate alkaline basalts in Shandong, North China. Chemical Geology, 2010, 273, 35-45.	3.3	180
248	Melting of enriched Archean subcontinental lithospheric mantle: Evidence from the ca. 1760Ma volcanic rocks of the Xiong'er Group, southern margin of the North China Craton. Precambrian Research, 2010, 182, 204-216.	2.7	160
249	Middle to late Jurassic felsic and mafic magmatism in southern Hunan province, southeast China: Implications for a continental arc to rifting. Lithos, 2009, 107, 185-204.	1.4	331
250	Jurassic sedimentary features and tectonic settings of southeastern China. Science in China Series D: Earth Sciences, 2009, 52, 1969-1978.	0.9	24
251	Early Cambrian ocean anoxia in South China. Nature, 2009, 459, E5-E6.	27.8	135
252	Pb–Pb dating of black shales from the Lower Cambrian and Neoproterozoic strata, South China. Chemie Der Erde, 2009, 69, 183-189.	2.0	22

#	Article	IF	CITATIONS
253	Palaeoceanographic redox environments for the lower Cambrian Hetang Formation in South China: Evidence from pyrite framboids, redox sensitive trace elements, and sponge biota occurrence. Palaeogeography, Palaeoclimatology, Palaeoecology, 2009, 271, 279-286.	2.3	137
254	How well do non-traditional stable isotope results compare between different laboratories: results from the interlaboratory comparison of boron isotope measurements. Journal of Analytical Atomic Spectrometry, 2009, 24, 825.	3.0	42
255	Dissolved inorganic carbon (DIC) and its carbon isotopic composition in sediment pore waters from the Shenhu area, northern South China Sea. Journal of Oceanography, 2008, 64, 303-310.	1.7	33
256	Geochemistry of pore waters from the Xisha Trough, northern South China Sea and their implications for gas hydrates. Journal of Oceanography, 2008, 64, 459-470.	1.7	19
257	The age and tectonic environment of the rhyolitic rocks on the western side of Wuyi Mountain, South China. Science in China Series D: Earth Sciences, 2008, 51, 1053-1063.	0.9	99
258	Boron isotopic fractionation in laboratory inorganic carbonate precipitation: evidence for the incorporation of B(OH)3 into carbonate. Science in China Series D: Earth Sciences, 2008, 51, 1776-1785.	0.9	15
259	Geochronology, geochemistry and Hf–Sr–Nd isotopic compositions of Huziyan mafic xenoliths, southern Hunan Province, South China: Petrogenesis and implications for lower crust evolution. Lithos, 2008, 102, 65-87.	1.4	72
260	Chemical and boron isotopic variations of tourmaline in the Hnilec granite-related hydrothermal system, Slovakia: Constraints on magmatic and metamorphic fluid evolution. Lithos, 2008, 106, 1-11.	1.4	78
261	Where was South China in the Rodinia supercontinent?. Precambrian Research, 2008, 164, 1-15.	2.7	281
262	Geochronology and geochemistry of Neoproterozoic mafic rocks from western Hunan, South China: implications for petrogenesis and post-orogenic extension. Geological Magazine, 2008, 145, .	1.5	109
263	Extreme enrichment of polymetallic Ni–Mo–PGE–Au in Lower Cambrian black shales of South China: An Os isotope and PGE geochemical investigation. Palaeogeography, Palaeoclimatology, Palaeoecology, 2007, 254, 217-228.	2.3	151
264	Trace and rare earth element geochemistry of phosphate nodules from the lower Cambrian black shale sequence in the Mufu Mountain of Nanjing, Jiangsu province, China. Chemical Geology, 2007, 244, 584-604.	3.3	133
265	Contrasting origins of late Mesozoic adakitic granitoids from the northwestern Jiaodong Peninsula, east China: implications for crustal thickening to delamination. Geological Magazine, 2007, 144, 619-631.	1.5	154
266	Petrogenesis of Late Jurassic Qianlishan granites and mafic dykes, Southeast China: implications for a back-arc extension setting. Geological Magazine, 2006, 143, 457-474.	1.5	112
267	Low-degree melting of a metasomatized lithospheric mantle for the origin of Cenozoic Yulong monzogranite-porphyry, east Tibet: Geochemical and Sr–Nd–Pb–Hf isotopic constraints. Earth and Planetary Science Letters, 2006, 241, 617-633.	4.4	214
268	Trace- and rare-earth element geochemistry and Pb–Pb dating of black shales and intercalated Ni–Mo–PGE–Au sulfide ores in Lower Cambrian strata, Yangtze Platform, South China. Mineralium Deposita, 2006, 41, 453-467.	4.1	126
269	Early J2 basalts in SE China: Incipience of large-scale late Mesozoic magmatism. Science in China Series D: Earth Sciences, 2006, 49, 796-815.	0.9	38
270	Petrogenesis of a Late Jurassic Peraluminous Volcanic Complex and its High-Mg, Potassic, Quenched Enclaves at Xiangshan, Southeast China. Journal of Petrology, 2005, 46, 1121-1154.	2.8	149

#	Article	IF	CITATIONS
271	Mobility of high field strength elements (HFSE) in magmatic-, metamorphic-, and submarine-hydrothermal systems. Physics and Chemistry of the Earth, 2005, 30, 1020-1029.	2.9	141
272	Mineral chemistry of the Qitianling granitoid and the Furong tin ore deposit in Hunan Province, South China: implication for the genesis of granite and related tin mineralization. European Journal of Mineralogy, 2005, 17, 635-648.	1.3	55
273	Two subgroups of A-type granites in the coastal area of Zhejiang and Fujian Provinces, SE China: age and geochemical constraints on their petrogenesis. Earth and Environmental Science Transactions of the Royal Society of Edinburgh, 2004, 95, 227-236.	0.3	56
274	Trace and rare-earth element geochemistry in tourmaline and cassiterite from the Yunlong tin deposit, Yunnan, China: implication for migmatitic–hydrothermal fluid evolution and ore genesis. Chemical Geology, 2004, 209, 193-213.	3.3	152
275	Paleoceangraphic significance of redox-sensitive metals of black shales in the basal Lower Cambrian Niutitang Formation in Guizhou Province, South China*. Progress in Natural Science: Materials International, 2004, 14, 152-157.	4.4	46
276	Re-Os isotopes and PGE geochemistry of black shales and intercalated Ni-Mo polymetallic sulfide bed from the Lower Cambrian Niutitang Formation, South China*. Progress in Natural Science: Materials International, 2003, 13, 788-794.	4.4	46
277	Pb-Pb isotope dating of black shales from the Lower Cambrian Niutitang Formation, Guizhou Province, South China*. Progress in Natural Science: Materials International, 2003, 13, 771-776.	4.4	19
278	Chemical and boron isotopic compositions of tourmaline from the Archean Big Bell and Mount Gibson gold deposits, Murchison Province, Yilgarn Craton, Western Australia. Chemical Geology, 2002, 188, 229-247.	3.3	83
279	Petrology and geochemistry of shoshonitic plutons from the western Kunlun orogenic belt, Xinjiang, northwestern China: implications for granitoid geneses. Lithos, 2002, 63, 165-187.	1.4	140
280	Origin of ore-forming fluids of the Dachang Sn-polymetallic ore deposit: Evidence from helium isotopes. Science Bulletin, 2002, 47, 1041-1045.	1.7	45
281	Sm-Nd dating of the giant Sullivan Pb-Zn-Ag deposit, British Columbia. Geology, 2000, 28, 751.	4.4	46
282	Chemical and Rb–Sr, Sm–Nd isotopic systematics of tourmaline from the Dachang Sn-polymetallic ore deposit, Guangxi Province, P.R. China. Chemical Geology, 1999, 157, 49-67.	3.3	101
283	Boron isotope systematics of tourmaline formation in the Sullivan Pb–Zn–Ag deposit, British Columbia, Canada. Chemical Geology, 1999, 158, 131-144.	3.3	59
284	Paragenesis and chemistry of multistage tourmaline formation in the Sullivan Pb-Zn-Ag deposit, British Columbia. Economic Geology, 1998, 93, 47-67.	3.8	66
285	Boron isotope systematics of tourmaline from granites and pegmatites: a synthesis. European Journal of Mineralogy, 1998, 10, 1253-1266.	1.3	97
286	Chemical and stable isotopic compositions of Proterozoic metamorphosed evaporites and associated tourmalines from the Houxianyu borate deposit, eastern Liaoning, China. Chemical Geology, 1997, 135, 189-211.	3.3	79
287	Silicon isotope geochemistry of the Sullivan Pb-Zn deposit, Canada; a preliminary study. Economic Geology, 1994, 89, 1623-1629.	3.8	30
288	Genesis of the Hermyingyi W–Sn deposit, Southern Myanmar, SE Asia: Constraints from fluid inclusion and multiple isotope (C, H, O, S, and Pb) studies. Mineralium Deposita, 0, , .	4.1	2